Reconstruction of Nanoscale Near Fields by Attosecond Streaking

Johannes Schötz, Benjamin Förg, Michael Förster, William A. Okell, Mark I. Stockman, Ferenc Krausz, Peter Hommelhoff, and Matthias F. Kling

(Invited Paper)

***Abstract*—Recent advances in attosecond science in combination with the well-established techniques of nanofabrication have led to the new research field of attosecond nanophysics. One central goal is the characterization and manipulation of electromagnetic fields on the attosecond and nanometer scale. This has so far remained challenging both theoretically and experimentally. One major obstacle is the inhomogeneity of the electric fields. We present a general model below, which allows the description of attosecond streaking in near fields. It allows the classification into different regimes as well as the reconstruction of the electric fields at the surface. In addition, we discuss the case of parallel polarization of the streaking fields to the surface, which has so far not been considered for attosecond streaking from metallic surfaces. Finally, we review recent measurements of the electric field and response function of a gold nanotaper. Our results are highly relevant for future attosecond streaking experiments in inhomogeneous fields.**

***Index Terms*—Ultrafast optics, near fields, nanotechnology.**

Manuscript received August 30, 2016; revised October 31, 2016; accepted October 31, 2016. Date of publication November 8, 2016; date of current version December 7, 2016. This work was supported in part by the Max Planck Society and the DFG through SPP1840 and in part by the Cluster of Excellence: Munich Centre for Advanced Photonics. The work of B. Förg was supported in part by the Marco Allione and Enzo Di Fabrizio via the King Abdullah University of Science and Technology and in part by the EU via the ERC Grant ATTOCO. The work of M. Förster and P. Hommelhoff was supported via the ERC Grant NearFieldAtto. The work of M. I. Stockman was supported in part by the Materials Sciences and Engineering Division of the Office of the Basic Energy Sciences, Office of Science, US Department of Energy under Grant DE-FG02-11ER46789 and in part by the Chemical Sciences, Biosciences and Geosciences Division of the Office of the Basic Energy Sciences, Office of Science, US Department of Energy under Grant DE FG02-01ER15213. The work of M. F. Kling was supported by the EU via the ERC Grant ATTOCO.

J. Schötz, B. Förg, F. Krausz, and M. F. Kling are with the Max-Planck-Institute of Quantum Optics, Garching D-85748, Germany, and also with the Physics Department, Ludwig-Maximilians-Universität München, Munich 80539, Germany (e-mail: johannes.schoetz@physik.uni-muenchen.de; benjamin.foerg@mpq.mpg.de; ferenc.krausz@mpq.mpg.de; matthias.kling@mpq.mpg.de).

M. Förster and P. Hommelhoff are with the Max-Planck-Institute of Quantum Optics, Garching D-85748, Germany, and also with the Department of Physics, Friedrich-Alexander Universität Erlangen-Nürnberg, Erlangen D-91058, Germany (e-mail: michael.foerster@fau.de; peter.hommelhoff@physik.uni-erlangen.de).

W. A. Okell is with the Max-Planck-Institute of Quantum Optics, Garching D-85748, Germany (e-mail: william.okell@mpq.mpg.de).

M. I. Stockman is with the Max-Planck-Institute of Quantum Optics, Garching D-85748, Germany, and also with the Department of Physics and Astronomy, Georgia State University, Atlanta, GA 30303 USA (e-mail: mstockman@gsu.edu).

Color versions of one or more of the figures in this paper are available online at http://ieeexplore.ieee.org.

Digital Object Identifier 10.1109/JSTQE.2016.2625046

I. Introduction

THE ability to create few-cycle laser pulses and to control their field on subcycle time scales [1]–[4] has enabled experimental studies of electron and nuclear dynamics on the attosecond time scale starting in the early 2000s. Attosecond science has been growing rapidly ever since [5]–[8]. While it was originally limited to atomic, molecular and bulk solids, recent advances have extended it to nanomaterials, which has led to the birth of the research field of attosecond nanophysics [9], [10]. By studying nanostructures with attosecond measurement tools, the natural time and length scale of the fastest electron processes are combined. Besides many useful applications in ultrafast sensing, microscopy and electron sources, the attosecond nanoscale control of light-matter interaction has the potential to ultimatively lead to the development of ultrafast light-driven electronics [11]–[14] with nanostructures. One common challenge in all applications is the characterization and control of nanoscale electric fields on the attosecond time scale.

Using attosecond streaking [15] for the characterization of electric near-fields around nanostructures on attosecond time scales has been proposed in 2007 [16], shortly after the first experimental realization of the technique in gases [17]. Extensive theoretical research followed [18]–[23]. It revealed that depending on how fast the electrons leave the near-fields, the relation of the measured streaking curve to the electric-field at the surface might differ drastically from the case of attosecond streaking in a homogeneous laser-focus. In a limiting case the electron might leave the near-field within a fraction of the field period. The streaking curve would then be directly proportional to the electric field at the surface, which has been termed "field probing" regime [16]. For classifying the different regimes, only recently the concept of a so-called adiabaticity parameter, originally introduced for strong-field photoemission from nanotips [24], was extended to attosecond streaking [25]. It is defined as the ratio of the escape time to the oscillation period. However the derivation was performed in a rather restrictive model for the temporal evolution of electric fields and therefore the question of applicability of the theory was not fully clear.

Experimentally only recently the realization of attosecond streaking measurements from a nanotaper were reported [25]. It was shown that the electric near-fields around the nanotaper could be reconstructed, thereby pushing the temporal resolution of electric field reconstruction from nanostructures from $\sim$50 fs

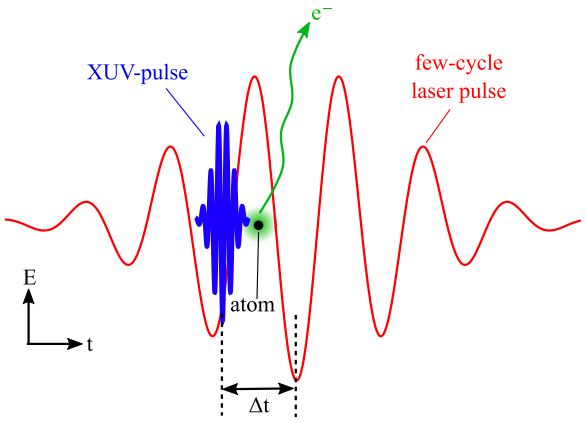

Fig. 1. Illustration of the basic principle of attosecond streaking: An electron is emitted by a weak attosecond-XUV pulse from an atom and subsequently accelerated by a laser pulse. The delay-dependent shift of the final electron velocity allows the reconstruction of the laser pulse as well as the attosecond XUV pulse.

[26] to the attosecond time scale. In addition, by comparison with gas streaking measurements, the response function of the taper could be extracted.

This paper is organized as follows. First, we theoretically consider the description of attosecond streaking in inhomogeneous near-fields around nanoobjects. We present a generalized model based on the theory in Refs. [7], [25], providing a clear distinction of the different regimes and analytic expressions for relating the near-fields at the surface to attosecond streaking measurements. Secondly, in a simple model, we discuss the attosecond delays in streaking from surfaces in the two extreme cases of grazing and normal incidence. Finally we review attosecond streaking measurements of near-fields around a nanotaper [25].

II. Attosecond Streaking

Attosecond streaking allows the reconstruction of electric fields with few attosecond precision. We first consider attosecond streaking in the classical case of a homogeneous field, in order to introduce the concept and some important relations, which we will use later. Then, we discuss the description of inhomogeneous near-fields at nano-objects. Finally, we derive a quantitative relation of the near-field and incident field to attosecond streaking measurement and work out the relevant parameter distinguishing different regimes of attosecond near-field streaking.

A. Attosecond Streaking in Homogeneous Fields

The principle of attosecond streaking is shown in Fig. 1. Attosecond streaking relies on the linear photoemission from an atom by an isolated weak attosecond pulse and the subsequent acceleration of the electron in the oscillating laser field of another, intense laser pulse. The typical photon energy of the isolated attosecond pulse lies in the extreme ultraviolet range (XUV, $\hbar\omega \sim 100$ eV). The initial kinetic energy E_{kin} of the electron is given by the difference of photon energy $\hbar\omega$ and the binding potential I_p. The acceleration of the electron in the electric field of the laser pulse changes its final kinetic energy. The change of the kinetic energy depends on the time of emission of the electron. The field strength of the laser pulse is generally chosen such that the electron energy is only slightly changed. By varying the delay Δt of the attosecond XUV pulse with respect to the laser pulse, the temporal structure of both pulses can be obtained from the change of the kinetic energy spectrum of the photoelectrons [15], [17].

In the framework of classical mechanics the dynamics of the attosecond streaking process is described by Newton's equation of motion:

$$\frac{\mathrm{d}\vec{v}}{\mathrm{d}t} = -\frac{e}{m} \cdot \vec{E}(t), \tag{1}$$

where $\vec{v}$, $-e$ and m is the electron velocity, charge and mass, respectively. We assume a spatially homogeneous electric field $\vec{E}(t)$ of the laser pulse. We neglect any static as well as magnetic fields. The final velocity v_{final} of an electron emitted at time t_0 with velocity $\vec{v}_0$ can be obtained by integrating Eq. 1 from t_0 to ∞ and using the relation of the vector potential $\vec{A}(t)$ to the electric field $\vec{A}(t) = -\int_{-\infty}^{t} E(t')\mathrm{d}t'$:

$$\vec{v}_{\mathrm{final}}(t_0) = \vec{v}_0 - \frac{e}{m} \cdot \vec{A}(t_0), \tag{2}$$

where we used $\vec{A}(\infty) = 0$ for an oscillating laser pulse. Taking the Fourier transform with respect to the delay t_0 and inverting the relation, the electric field in the frequency domain $\vec{E}(\omega)$ can be obtained:

$$\vec{E}(\omega) = -i\omega \cdot \vec{v}_{\mathrm{final}}(\omega) \cdot \frac{m}{e}. \tag{3}$$

Above and in the following we use the convention that the use of the temporal or frequency domain is indicated by the variables t or ω, while the symbols for the physical quantities stay the same. In the case of spatially inhomogeneous fields the total electric field consists of the incident field and the localized, excited near-fields and is therefore position-dependent. The experimentally measurable change of the electron velocity will yield some effective field $E_{\mathrm{eff}}(\omega)$, which has to be related theoretically to the actual near- and incident field. In order to do so, we have to consider the light interaction with nanoparticles.

B. Description of Near-Fields at Nanoparticles

Nanostructures exhibit unique features in the interaction with light. The evanescent electric fields near nanoobjects (near-fields) show an enhancement of the electric field strength up to several orders of magnitude and confinement down to few nm, well below the diffraction limit of light. This is illustrated in Fig. 2(a), where the maximum electric field strength around a gold nanotip is shown, computed by a commercial finite-difference time-domain solver (Lumerical Solutions, FDTD 8.9). The field strength is normalized by the strength of the incident laser pulse. It is given by a 4.5 fs (intensity-FWHM) laser pulse centred at a wavelength of 750 nm and is polarized parallel to the nanotip. Both field enhancement and confinement at the tip apex are clearly visible. At the front side of the nanotip the near-field also varies on a subwavelength scale but is reduced in strength.

It is useful to make the description of the electric near-fields around a given nano-object independent of the temporal struc-

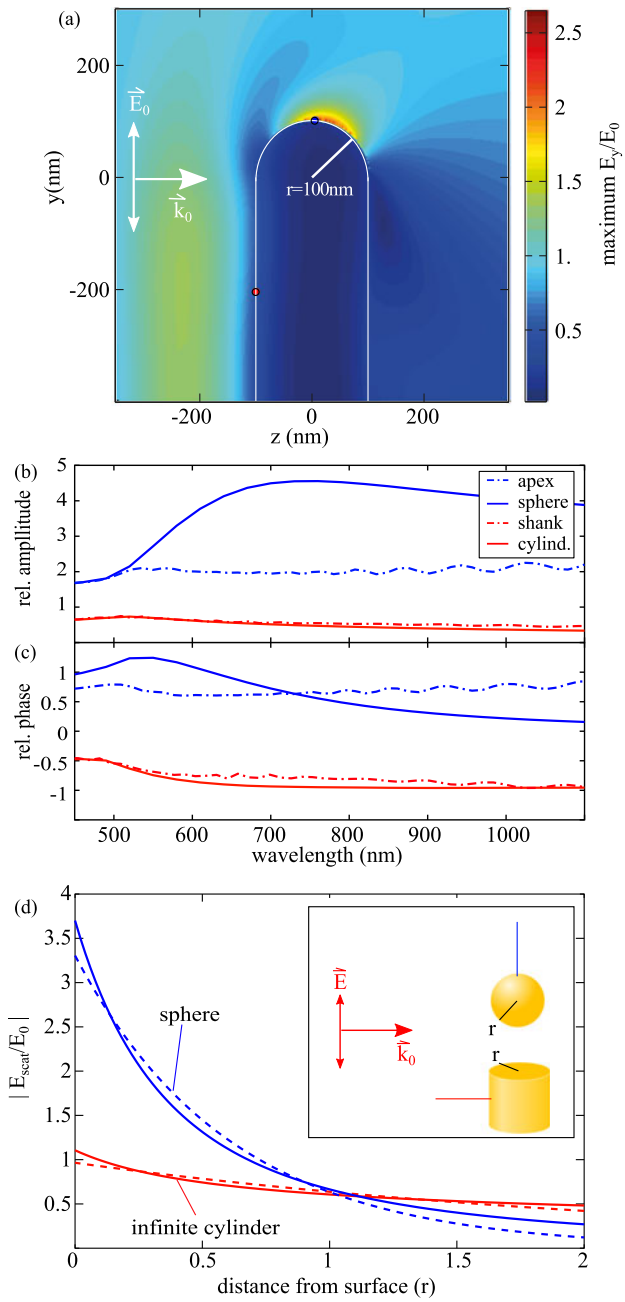

Fig. 2. Inhomogeneous near-fields around nanostructures. (a) Maximum electric field strength around a gold nanotip for a 4.5 fs pulse centred at a wavelength of 750 nm calculated by the FDTD method. Field component parallel to the nanotip axis is shown and normalized to the incident field. Amplitude (b) and phase (c) of the response function of the points shown in (a) (blue dashed-dotted: apex, red dashed-dotted: shank) and for the pole of a sphere (blue solid) and the front of an infinite cylinder (red solid) with the same radius. (d) Fit of the scattered near-fields by a decaying exponential for the pole of a sphere and the front of an infinite cylinder, as shown in the inset.

ture of the incident field. Therefore the concept of response functions is introduced in the following. In the framework of linear Maxwell's equations in the frequency domain, the total field at a given point depends linearly on the excitation field: $\vec{E_{\rm tot}}(\vec{r},\omega) = R(\vec{r},\omega)\cdot\vec{E_0}(\omega)$. The response function $R(\vec{r},\omega)$ is in principle represented by a 3 × 3-matrix, however fixing the polarization of the incident field and considering only a single component of the total field, reduces it to a scalar function. Fig. 2(b) and (c) show the absolute value and phase of the response function for the red and blue points shown in a) (apex: blue dashed-dotted, shank: red dashed-dotted) and both field components parallel to the nanotip axis. The incident Gaussian beam is focused onto the nanotip apex with a waist of 3 μm. For comparison the response function of the pole of a gold nanosphere (blue) and the frontside of an infinite cylinder (red) calculated by Mie-theory (MatScat [27]) are shown. The sphere shows a significantly higher field enhancement than the apex and yields only roughly a similar positive phase. The response functions of shank and infinite cylinder in contrast show a good agreement, both yielding a decrease in field strength and a negative phase. We note for later reference that the fields at the apex and shank obey different boundary conditions (see e.g. [28]), which is connected to the different behaviour of the response function. At the apex, the incident field is polarized normal to the surface, yielding the boundary condition $\epsilon_1 E_1 = \epsilon_2 E_2$ and a sudden change of the electric field at the surface. On the shank however, the incident field is parallel to the surface, resulting in $E_1 = E_2$ and the continuity of the fields across the surface, which can be seen in Fig. 2(a). In all response functions the transition to the free-electron-like behaviour of the dielectric function of gold (taken from [29]) at 500 nm is visible. The goal of attosecond near-field sampling is not only to measure the total electric field at a nanostructure, but to extract the response function of the nanosample. This requires knowledge of the incident field, which for example can be obtained by streaking in noble gases.

In order to obtain a general description of near-fields, the spatial dependence has to be considered. As usual in scattering theory, we divide the total field $E_{\rm tot}$ into incident E_0 and scattered fields $E_{\rm scatt}$ [30]:

$$E_{\rm tot} = E_0 + E_{\rm scatt}. \tag{4}$$

A fundamental aspect of nano-optics is that the presence of nano-objects allows to confine light below the diffraction limit [28]. A general solution for the scattered field of Maxwell's equations is of the form $e^{ik_x\cdot x + ik_y\cdot y - i\omega t}$ (setting $k_z = 0$ for simplicity). Due to the nanostructure one component of the wavevector can be purely imaginary, while still fulfilling the dispersion relation of free space $k_x^2 + k_y^2 = \frac{\omega^2}{c^2}$, where c is the speed of light. This can be realized by increasing the other component beyond ω/c. It is the complex component that describes the field confinement. It can be related to the near-field decay-length l_f by $k_i = i\cdot\frac{1}{l_f}$. Thus the near-fields around nanostructures are generally described by a superposition of decaying fields of the form $E_{\rm scatt} \propto e^{-x/l_f}$. Fig. 2(d) shows the absolute values of the scattered fields away from the pole of a sphere (blue) and the front side of a cylinder (red), as shown by the inset. The dashed lines show a fit of the scattered fields to an exponential function $a\cdot e^{-b\cdot x}$, where a and b are complex values. Both cases are fairly well approximated by single exponential decaying functions, with better agreement for the sphere. While the pole shows almost a purely exponential decay, the fields of the cylinder also shows some propagating character. We mention that the decay-length is typically on the order of the size of the geometric features of the nanostructure. Having worked

out the general spatial dependence of near-fields, we are ready to consider attosecond streaking in such fields.

C. Attosecond Streaking in Inhomogeneous Fields

The model presented in the following section is a generalization of the models presented in Refs. [7], [25], thereby significantly increasing the applicability to experiments. For describing a general near-field, we consider a one-dimensional model, taking into account the decay length of the central spectral component of the laser pulse and write the total field as:

$$E_{\mathrm{tot}}(x,t) = E_0(t) + E_{\mathrm{scatt}}(t)\cdot\exp(-x/l_f), \tag{5}$$

with a homogeneous incident field E_0 and the scattered field E_{scatt}. The problem in solving Eq. 1 is the spatial dependence of the field. Recalling that the intensity of the laser pulse is chosen such that the variation of the kinetic energy is just a small fraction of the total kinetic energy, we can expand the electric field E, the electron velocity v and position x in terms of a small parameter ϵ as follows:

$$E = \epsilon\cdot E_{\mathrm{tot}} \tag{6}$$

$$v(t) = v_0 + \epsilon\cdot v_1(t) + \mathcal{O}(\epsilon^2) \tag{7}$$

$$x(t) = v_0\cdot(t-t_0) + \epsilon\cdot\int_{t_0}^{t} v_1(t)\mathrm{d}t + \mathcal{O}(\epsilon^2), \tag{8}$$

where we implicitly solved the zeroth order equation of motion. Basically in zeroth order, when considering the position, we are ignoring the change of velocity of the electron. In first order the equation of motion reads:

$$\frac{\mathrm{d}v}{\mathrm{d}t} = -\frac{e}{m}\Big[E_0(t) + E_{\mathrm{scatt}}(t)\cdot\exp\Big(-v_0(t-t_0)/l_f\Big)\Big]. \tag{9}$$

The r.h.s. of Eq. 9 has only a temporal dependence. The electron thus experiences an effective field with only temporal dependence and the equation of motion is solved analogously to Eqs. 1, 2, 3. The effective field as measured by attosecond streaking in an inhomogeneous field relates to the incident and scattered fields by Fourier transforming the above expression:

$$\begin{aligned} E_{\mathrm{eff}}(\omega) &= \frac{E_0(\omega)+E_{\mathrm{scatt}}(\omega)}{1-i\frac{v_0}{l_f\cdot\omega}} + \frac{E_0(\omega)}{1+i\frac{l_f\cdot\omega}{v_0}} \\ &= \frac{E_{\mathrm{surf}}(\omega)}{1-i\frac{1}{2\pi\delta(\omega)}} + \frac{E_0(\omega)}{1+i2\pi\delta(\omega)}, \end{aligned} \tag{10}$$

where we have used the field at the surface $E_{\mathrm{surf}} = E_0 + E_{\mathrm{scatt}}(x=0)$ and introduced the adiabaticity parameter δ [25]:

$$\delta(\omega) = \frac{l_f}{v_0\cdot T_0} = \frac{T_{\mathrm{esc}}}{T_0}, \tag{11}$$

where T_{esc} is the escape time from the near-field defined as $T_{\mathrm{esc}} = l_f/v_0$. For details of the derivation and the relation to the adiabaticity parameter in strong-field photoemission as well as to a generalized adiabaticity parameter, we refer to the appendix. A schematic illustration of the electron propagation in near-fields for different adiabaticity parameters is shown in Fig. 3(a). We note that the relation of the effective field to the surface and incident fields only depends on the adiabaticity parameter.

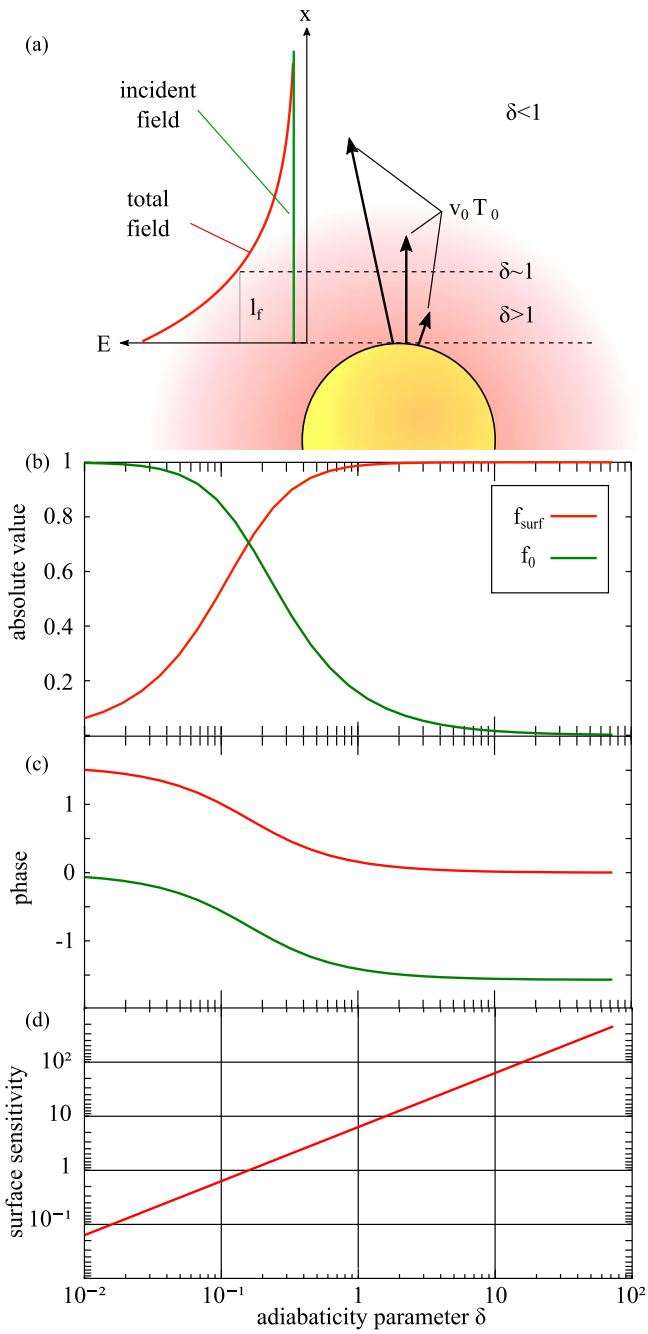

Fig. 3. (a) Illustration of the relation between field decay length and electron propagation for different adiabaticity parameters δ. Depending on the distance that the electron travels within one optical period $v_0\cdot T_0$ different streaking regimes are realized. The absolute value and the phase of the functions f_{surf} and f_0 are shown in (b) and (c). The surface sensitivity, the ratio of the absolute value between f_{surf} and f_0 is shown in (d).

We call the functions determining the proportionality of E_{eff} to E_{surf} the surface field function $f_{\mathrm{surf}}(\delta)$ and E_{eff} to E_0 the incident field function $f_0(\delta)$.

$$f_{\mathrm{surf}}(\delta) = \left(1 - i\cdot\frac{1}{2\pi\cdot\delta}\right)^{-1} \tag{12}$$

$$f_0(\delta) = (1 + i\cdot 2\pi\cdot\delta)^{-1}. \tag{13}$$

These functions contain the information about the proportionality and the relative phase of the measured effective field to

the surface field and incident field with varying adiabaticity parameter. The absolute value and phase of the two functions are shown in Fig. 3(b) and (c). By examining the behaviour of these functions we can identify three different regimes of attosecond streaking in near-fields:

1) "ponderomotive regime" $\delta > 1$: The escape time of the electron from the near-field is much larger than the period of the field. The electron experiences a quasi homogeneous field during an optical cylce. The measured field E_{eff} is quasi identical to the surface field E_{surf}, as f_{surf} has an amplitude of almost unity and zero phase, while f_0 has nearly zero amplitude.
2) "intermediate regime" $0.05 < \delta < 1$: The electron starts to experience the inhomogeneity during one cycle. The impact of the surface field function decreases while the incident field function increases in amplitude. Moreover the surface field function starts to shift out of phase while the incident field function, which was shifted by $-\pi$, starts to get in phase.
3) "field probing regime" $\delta < 0.05$: The electron leaves the near-field almost instantaneously in a fraction of a cycle and sees a quasi-static near-field. The naming has been introduced in Ref. [16]. As the phase of the surface field function is π out of phase with E_{eff}, the measured streaking trace is directly proportional to the surface field, if we ignore the incident field. However we note that the amplitude of the surface field function approaches zero while the incident field function approaches unity and is in phase. The actual measured quantity will thus depend on the ratio of the field strength of surface field and incident field and the naming of the regime might have to be reconsidered.

The limitation of the field probing regime is further illustrated in Fig. 3(d) where the surface field sensitivity $s = |f_{\mathrm{surf}}/f_0|$ is shown. If s multiplied by the field enhancement $|E_{\mathrm{surf}}(\omega)/E_0(\omega)|$ is greater 1, the surface field dominates the measured effective field, otherwise the incident field. In order to probe the surface field in the "field probing regime" the minimum possible field enhancement is greater than 10. This is illustrated in the extreme, where we shrink the nanosystem to a single atom or molecule where the incident laser pulse excites a polarization field.

Knowledge of the adiabaticity parameter allows reconstruction of the surface response function $R(\omega) = \frac{E(\omega)}{E_0(\omega)}$ from the measured effective and incident fields:

$$R_{\mathrm{surf}}(\omega) = \frac{1}{f_{\mathrm{surf}}(\delta(\omega))} \cdot \left(\frac{E_{\mathrm{eff}}(\omega)}{E_0(\omega)} - f_0(\delta(\omega)) \right). \quad (14)$$

The presented model can in principle be extended to complex near-field decay length l_f and even a superposition of near-field components with different decay-lengths for a more precise description of the attosecond streaking process if the specific near-fields are known. However, such an extension is less general and more complex without offering additional insight and is therefore not discussed here.

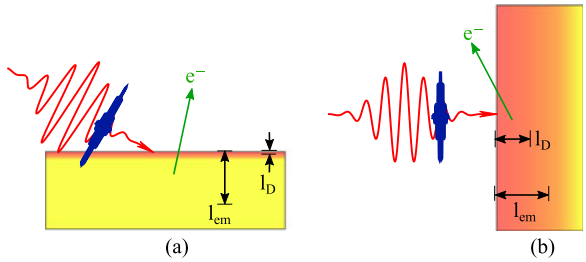

Fig. 4. Illustration of the different boundary conditions encountered in attosecond streaking from solids and its effect on streaking delays in a simple model: (a) grazing incidence geometry where the electric field is damped on a few angstrom length scale. Electrons originating from inside the solid only feel the electric field as they penetrate the surface. (b) normal incidence geometry: Since the normal component of the electric field is continous and only decays with the field decay length (few nanometers), all the electrons from within the emission depth feel a similar electric field as those having crossed the surface.

III. Streaking Time Delays

Attosecond streaking received a lot of attention, when it was applied to measuring photoemission from several different initial states of the same system simultaneously. It was found that relative shifts of the streaking curves for different initial states of atoms or solids can be on the order of 10-100 as [31]–[34]. Such shifts are called relative streaking delays. They can be interpreted as the photoemission process not being instantaneous but occuring with some time delay τ_s with respect to the incident laser [34]. For the cases discussed here this means that also the reconstructed electric field will be shifted with respect to the actual electric field of the laser pulse. The absolute streaking delays are not accessible experimentally and have to be extracted from theory. For experiments, where electric fields obtained from streaking from gases to streaking from nanoobjects are compared, an estimation of the effect of absolute time delays is necessary. We note that closely related time delays are found in another attosecond measurement technique [35], the so called RABITT-method [36], enlarging the amount of relevant literature [35], [37]–[39].

For gases a number of theoretical studies exist and we refer to [34] for a review. In a recent study on neon for photon energies above 70 eV, the energy range relevant for the experimental results presented later, the absolute streaking time shift lies below 10 as [40].

For solid surfaces the situation is more complicated. We want to point out that there are two different extreme cases of geometries to consider in streaking from metal nanobjects. These are closely related to the two different boundary conditions of the electric field discussed in Sec. II-B. So far only one of them is dealt with in studies related to photoemission from extended solid surfaces, despite the large amount of theoretical studies [41]–[46]. The reason is that all related experiments up to now were performed on flat macroscopic surfaces. The two different geometries are illustrated in Fig. 4(a) and (b). In both cases the electrons are detected at the top.

The first one shows the usual situation. Both laser pulses illuminate the surface under grazing incidence. The optical pulse is shielded on the length scale of the electrostatic screening length l_D inside the solid, which is for metals on the order of

a single atomic layer. The field strength of the field inside the material relative to the surface field is given by the Maxwell boundary condition for grazing incidence (see Sec. II-B). It is given by $1/|\epsilon|$, which is around 4% for gold at 800 nm [29]. Earlier streaking experiments on a tungsten surface with varying Mg-overlayer thickness could deduce a screening length of $\sim$1 Å [47]. The XUV beam on the other hand can penetrate into the solid, leading to photoemission not only from the surface but also from within the solid. The emission depth l_{em} from which electrons can escape the surface is mainly limited by the length scale of inelastic scattering, the so called inelastic mean free path, which is usually larger than the screening length. In this geometry, electrons which are excited within the metal take some time to reach the surface, only then they start to experience the streaking field. For electron energies below 30 eV a recent experimental study comparing argon gas with a macroscopic flat gold surface by using RABITT, yielded relative delays on the order of 100 as [39]. For higher energies, the delay is generally expected to be smaller. An estimate of the absolute streaking delay is given by the ratio of the average escape depth and the electron velocity inside the metal, giving around 60 as [48], [49] ignoring details of the bandstructure.

The situation is different for the geometry depicted in Fig. 4(b). There the incident electric field is polarized parallel to the surface. Now we only consider the electrons that are emitted quasi-parallel to the surface, since only if they propagate parallel to the polarization direction they will experience a significant energy shift due to the streaking field. The electric field is continuous across the surface and only decays with the screening length (30 nm [29]). This is much larger then the emission depth and therefore all electrons feel the streaking field from the time of birth.

Although this is a very crude description, which ignores any quantum effects, we expect the absolute streaking time delay for this geometry to be below 10 as. Since there are to date no theoretical studies for this second geometry, we assume as a working hypothesis negligible streaking delays, but keeping in mind that when comparing the electric fields reconstructed from gases and nanoobjects, there might be systematic errors on the order of $\sim$50 as for the first and $\sim$10 as for the latter geometry. Only recently a RABITT experiment compared attosecond time delays in photoemission for grazing incidence and quasi normal incidence and strongly supported the above simple ballistic electron transport model in the framework of macroscopic Maxwell's equations [50]. For nanotips both boundary conditions are found, the grazing incidence geometry for electrons emitted from the nanotaper apex and the normal incidence geometry for the nanotaper side. As will be discussed below, for the measurements in this work, only the latter has to be considered and therefore merely minor streaking delays are to be expected.

IV. Experimental Setup for Attosecond Streaking from a Nanotaper

The laser and the experimental setup used for the measurements presented in this paper are shown Fig. 5(a) and (b).

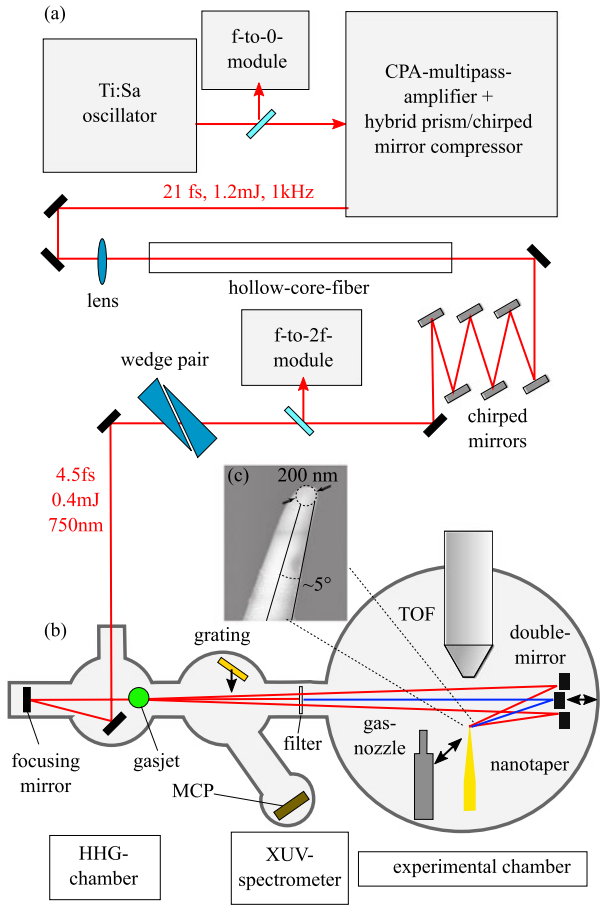

Fig. 5. Scheme of the experimental setup used in the experiments (see text for detais): (a) The laser setup. (b) The experimental chamber. (c) SEM-picture of a nanotaper.

The laser setup consists of a Ti:sapphire oscillator (Femtolasers Rainbow), generating $\sim$7 fs pulses with 3.5 nJ at 70 MHz centered at 800 nm. The carrier-envelope phase (CEP) of the pulses is measured by a f-to-0 module [51], which provides feedback for the CEP-stabilization (Menlo Systems) inside the oscillator. The oscillator output is subsequently amplified in a multipass chirped-pulse amplifier (FemtoPower Compact Pro), yielding 21 fs pulses with 2 mJ at 1 kHz. The pulses are then focused into a hollow-core fiber filled with 2 bar neon for spectral broadening via self-phase modulation and self-steepening. Afterwards the dispersion of the pulses is compensated by chirped mirrors. A part of the output beam is sent into the f-to-2f-module for measuring the CEP of the amplified short pulses. A feedback is provided to one prism in the pulse compressor after the CPA-multipass amplifier to compensate for slow drifts of the CEP. A wedge pair serves for fine tuning of the dispersion. Finally pulses with a duration of $\sim$ 4.5 fs and $\sim$400 μJ are sent to the experimental chamber. There the laser pulses are focused into a neon gas jet for high-harmonic-generation (HHG) with an intensity of $\sim 5 \cdot 10^{14}$ W/cm, where extreme-ultraviolet (XUV) pulses are generated. The subsequent spectrometer section allows for the spectral characterization of the generated XUV-pulses. A two-part filter made of material which is only transmissive for either IR (nitrocellulose pellicle) or XUV (Zr

foil) is used to spatially separate the fundamental laser pulse and the XUV-light. In the experimental chamber a two-part mirror is used to focus the pulses onto the streaking targets. The inner part can be moved by a closed-loop piezo stage (PI P-752) relative to the outer mirror, thereby reproducibly creating a delay between the two pulses. The double mirror has a special coating selecting a spectral range of 7 eV centered around 93 eV, which defines the energy range of the final isolated attosecond pulse. The streaking targets consist of a nanotip and a gas nozzle mounted on a 3D-translation stage, which allows placing either target in the focus. The gas nozzle is used to optimize the generation of isolated attosecond pulses and the attosecond streaking and it also serves as a measurement of the incident field for the later measurements on the nanotips. The photoemitted electrons are measured by a time-of-flight spectrometer (TOF). The timing of the electron signals is recorded by a multiscaler card.

Fig. 5(c) shows an SEM image of a gold nanotaper used in the experiments. It is produced by the lamellae drop-off technique [52]. The employed nanotapers usually have a radius of $\sim$100 nm and a small full opening angle of around 10°. Therefore the tip geometry for the electric field calculations shown in Fig. 2 matches the tips used in the experiment fairly well.

The attosecond streaking experiments are performed in neon and the nanotaper under the same laser conditions. The electron countrate from strong-field photoemitted electrons from the nanotaper, which is highly sensitive to the field enhancement at the nanotip apex, is used to ensure reproducible positioning of the nanotaper in the IR- and XUV-focii (size $\sim$15 μm and $\sim$3 μm respectively).

In order to not destroy the nanotip samples the laser intensity should not exceed the damage threshold. On the other hand, the intensity has to be high enough to yield streaking amplitudes on the order of few eV. Using Eq. 2 and the parameters of our experiment a minimum intensity of $\sim 2 \cdot 10^{11}$ W/cm^2 is obtained. This is below the damage thresholds for surfaces [53] and even clearer below that of nanotips [54]. Laser irradiation might lead to a slight smearing of the Fermi edge [55], [56], which is however below the resolution of our experiment.

V. Experimental Results for Attosecond Streaking from a Nanotaper

An experimental streaking spectrogram, the electron kinetic energy spectrum for different delay steps, obtained from a nanotaper is shown in Fig. 6(a) together with the neon gas reference spectrogram b) taken under the same laser conditions. Clear oscillations can be observed in both spectrograms and close inspection shows a time shift between the oscillation. In order to quantify the shift of the two spectrograms, streaking curves have to be extracted from the spectrograms. The streaking spectrogram from neon shows a clear, nearly Gaussian kinetic energy spectrum for each delay step. By contrast, for the nanotaper the spectrum is significantly broadened and no clear peak shape in discernible below the cutoff of the spectrum. This could be due to inelastic scattering of the XUV-emitted electrons with surface plasmons [57]–[59]. However the statistics are too low to clearly discern plasmon satellites. The broadened spectrum together with low statistics prohibits standard retrieval methods

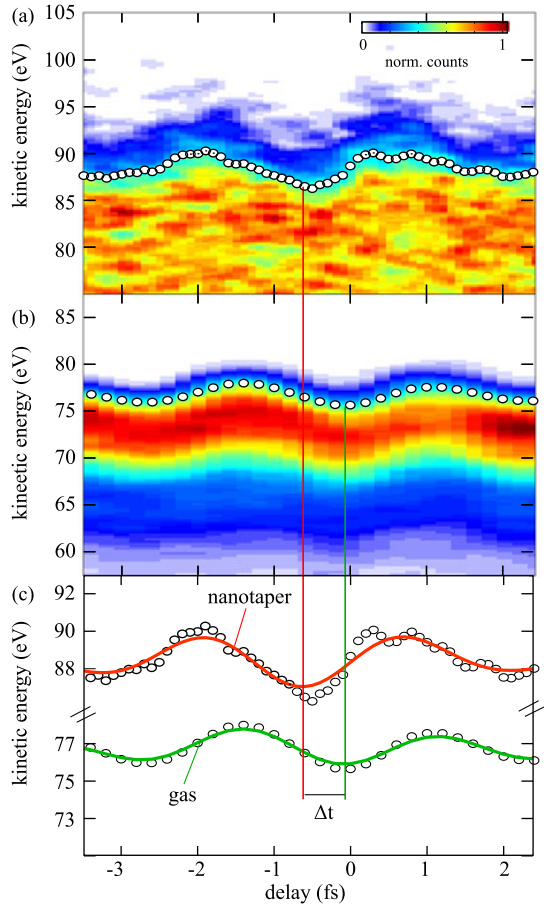

Fig. 6. Experimental results: Streaking curve from a gold nanotaper (a) and neon gas (b) under the same laser conditions. (c) Extracted streaking curves by applying a Fermi-fit to the cutoff region of the spectra (dots) and the Fourier-filtered streaking curve (solid line). A shift between the two curves is clearly visible.

[60] of attosecond streaking curves used in earlier analysis of attosecond streaking from solids. We therefore concentrate on the high-energy cutoff of the spectra, to which we fit a Fermi function for each delay. The turning points of the Fermi function are taken to define the raw streaking curve (dots). For consistency the same analysis has been applied to the gas streaking. There it could be shown [25] that the extracted streaking curves are in very good agreement with the FROG-CRAB method [60].

Remarkably, the streaking trace from the nanotaper is relatively homogeneous. From the theoretical calculation of the electric fields around the nanotaper (Fig. 2) two different streaking curves with different oscillation amplitudes and phases are expected, if contributions of both the nanotaper and the nanotip apex were visible. Comparing the area of the enhanced field with the area of the nanotaper side illuminated by the XUV-beam, we can conclude that the apex contribution is not visible with the limited statistics in our measurements. This is further supported by scanning the nanotaper through the XUV-focus. The position-dependent countrate from XUV-photoemission practically shows the outline of the nanotaper. Furthermore, Monte-Carlo simulations of the streaking traces support this assumption [25]. We thus conclude that the streaking spectrogram is constituted by electrons originating from the nanotaper side.

In order to remove noise, the curves are Fourier transformed. Then a lowpass filter is applied, removing all spectral components below 400 nm with a linear increase of the transmission filter to unity at 450 nm. These spectral components were not present in the incident optical laser pulse and can therefore be considered noise. Finally, the curves are transformed back into the time-domain. The resulting streaking curves are shown in Fig. 6(c) as solid lines. Now, a clear time shift Δt is visible, here about ∼500 as. In order to obtain the effective field E_{eff} and the incident field E_0, we directly use the streaking curves $T_{\text{kin}}(t_0)$ from the gas and nanotaper:

$$E_{\text{eff}/0}(t_0) = \frac{1}{2e}\frac{\sqrt{2m}}{\sqrt{T_{\text{kin}}(t_0)}}\frac{\partial T_{\text{kin}}(t_0)}{\partial t_0} \tag{15}$$

For the calculation of the derivative the lowpass-filtered curve in the Fourier-domain is used. In order to relate the effective field reconstructed from the nanotaper streaking to the surface field and the incident field, the streaking regime has to be examined. For this we use the theory laid out in section II. The electron velocity at a kinetic energy of 100 eV is approximately given by $6\frac{nm}{fs}$. From the SEM pictures of the nanotaper [see Fig. 5(c)], the geometric dimensions and the resulting field decay-length can be estimated to be on the order of ∼50-100 nm. Taking into account an oscillation period T_0 between 1.5 fs and 3 fs for the covered spectrum, we obtain an adiabaticity parameter δ between ∼2.5-10. This is still in the ponderomotive regime, even though the near-fields around the nanotaper change on a few nanometer length scale. In the reconstruction we can therefore to a very good approximation set $f_0 = 0$ and $f_{\text{surf}} = 1$ and take E_{eff} to be the surface field E_{surf}.

The amplitude and phase of the reconstructed response function of the nanotaper is shown in Fig. 7(a) and (b), by analysing a set of measurement taken on different days. The response function $E_{surf}(\omega)/E_0(\omega)$ is calculated from the streaking curves with the help of Eq. 3 and Fourier-Transform. The raw datapoints are shown as crosses. Their position on the wavelength-axis depends on the delay range covered by the individual streaking scan as well as on the delay stepsize. A mean response function is extracted by averaging the linearly interpolated responses from different scans at equally spaced wavelength values (dots) together with the corresponding standard deviation (errorbars). The individual scans are weighted by the total number of electron counts. The green areas show the expectation for the response function obtained by averaging the calculated reponse from a tapered nanowire. An apex radius of 50 nm and full opening angle of 10° has been assumed. The response is averaged over 10000 points on the surface of the nanotaper, with a distribution given by the profile of the XUV-beam that hits the nanotaper. The width of the green area corresponds to the standard deviation. The amplitude shows good agreement with the theoretical expectation. The experimentally extracted phase seems to be slightly shifted with respect to theory, but still shows decent agreement considering the width of reconstructed and theoretical response. Fig. 7(c) shows the temporal evolution of the reconstructed electric field (red solid line) from the nanotaper measurements shown in Fig. 6 together with the expectation (green area), calculated by using the extracted incident electric field and the amplitude and phase of the theoretical expectation shown in a) and b). There is very good agreement, illustrating successful implementation of the near-field sampling. By measuring the response function, the electric field for any incident laser pulse can in principle be predicted.

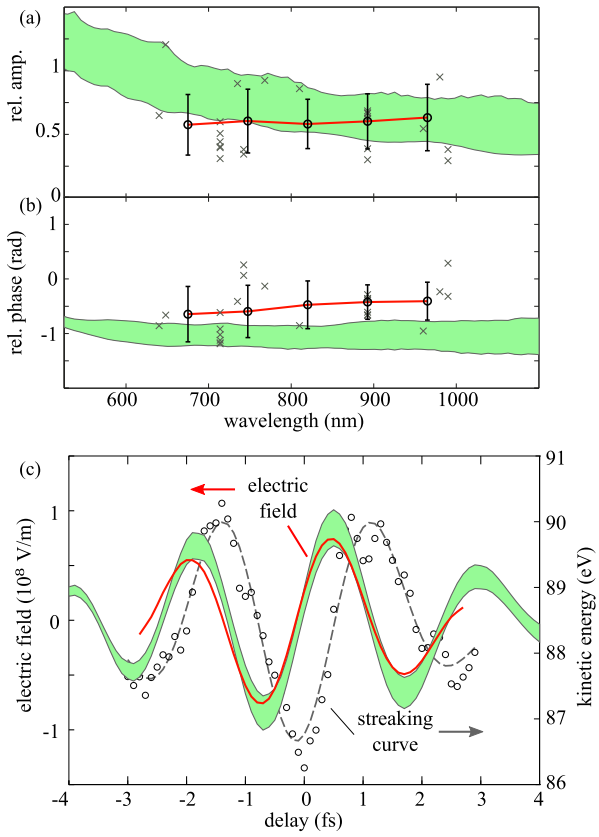

Fig. 7. Analysis of the experimental results: (a) and (b) show the amplitude and phase of the response function of the nanotip. Crosses show single datapoints from individual measurements. The dots show the average of all datapoints, the green area indicates the expected response function calculated by averaging the response of the illuminated surface area of a nanotaper. (c) Shows the extracted field for the dataset shown in Fig. 6(a). The green area represents the expectation for the electric field by using the input field in Fig. 6(b) and the averaged response function of (a) and (b). (a) and (b) adapted from Ref. [25], (c) adapted from Ref. [10].

VI. Conclusion and Outlook

We have presented a general model for attosecond streaking in near-fields, which is of high relevance for future attosecond experiments on nanostructures. We identify the adiabaticity parameter δ, defined as the ratio of escape time of the electron from the near-field to the oscillation period, as the relevant parameter for classifying three different regimes of attosecond streaking. In terms of this parameter, the model furthermore provides quantitative expressions relating attosecond streaking curves obtained from experiments to the surface near-field and response function. In the future, by changing the XUV energies and with this the streaking regime, it might be possible to obtain information on the spatial characteristics of the near-fields.

Moreover we identified two different photoemission geometries, which can be found in attosecond experiments from metal surfaces in connection with absolute photoemission time delays.

Usually both cases are encountered simultaneously in streaking experiments on nanostructures. For laser pulses with normal incidence and photoemission close to parallel to the surface, the electric field is quasi homogeneous over the emission depth. From simple considerations, it could be concluded that the delays due to electron propagation within the solid should be absent. Future more elaborate theoretical studies are however highly desirable.

Finally, we presented experimental attosecond streaking experiments in the near-field of a gold nanotaper. With the help of the theory presented in the first part, we are able to extract the electric near-field on the surface of the nanotaper with attosecond resolution. The demonstration of the different regimes of attosecond streaking in near-fields derived in the first part of the paper are left to future experiments as well as the measurements of single hotspots such as the nanotaper apex. Finally, by comparing the nanotaper results with the attosecond streaking experiments on neon under the same laser conditions, we demonstrate the ability to extract the response function of the nanotaper. The results are compared to theoretical expectations and generally good agreement is found. The measurement of the response function is of high relevance for any ultrafast application, because the temporal evolution of the near-field for any incident laser pulse can be predicted. Combining our approach with photoemission electron microscopes (PEEM), could give access to the attosecond fields on a nanometer scale, without prior knowledge of the geomtery of the nanostructure [16]. This will allow building more complex and functional nanostructures and enable the development of field-driven electronics.

Appendix
Derivation of the Extraction Function

By expressing the effective field of Eq. 9 in the Fourier representation of the the incident and scattered fields, we obtain:

$$E_{\mathrm{eff}}(t) = \int E_0(w)e^{-i\omega t} + E_{\mathrm{scatt}}(\omega)e^{-i\omega t - \frac{v_0}{l_f}\cdot(t-t_0)}\mathrm{d}\omega, \tag{16}$$

where we put the temporally decaying term under the integral. This expression can easily be integrated to yield:

$$\int_{t_0}^{\infty} E_{\mathrm{eff}}(t)\mathrm{d}t = \int \mathrm{d}\omega \frac{E_0(\omega)}{-i\omega}e^{-i\omega t_0} + \frac{E_{\mathrm{scatt}}(\omega)}{-i\omega - \frac{v_0}{l_f}}e^{-i\omega\cdot t_0}. \tag{17}$$

At $t = \infty$ the integral over t of the first term is zero for the same reason as in Eq. 2. The second term is zero, because of the exponential decay. Note that in the final expression the exponential decaying part has disappeared from the exponential of the second term. This leaves us with

$$\begin{aligned} E_{\mathrm{eff}}(\omega) &= -i\omega\left(\frac{E_0(\omega)}{-i\omega} + \frac{E_{\mathrm{scatt}}(\omega)}{-i\omega - \frac{v_0}{l_f}}\right) \\ &= -i\omega\frac{\left(-i\omega - \frac{v_0}{l_f}\right)\cdot E_0(\omega) - i\omega\cdot E_{\mathrm{scatt}}(\omega)}{-i\omega\cdot\left(-i\omega - \frac{v_0}{l_f}\right)} \\ &= \frac{-i\omega(E_0(\omega) + E_{\mathrm{scatt}}(\omega))}{-i\omega - \frac{v_0}{l_f}} + \frac{\left(-\frac{v_0}{l_f}\right)\cdot E_0(\omega)}{-i\omega - \frac{v_0}{l_f}} \end{aligned} \tag{18}$$

from which Eq. 10 follows immediately. Concerning the adiabaticity parameter $\delta = \frac{l_f}{v_0\cdot T_0}$, we note that in strong-field photoemission in inhomogeneous fields another adiabaticity parameter δ_{sf} has been identified $\delta_{\mathrm{sf}} = \frac{l_f}{l_q}$ in Ref. [24], where l_q is the quiver amplitude of an electron in a homogeneous field. δ_{sf} follows directly from Newton's equation of motion with an inhomogeneous near-field:

$$\frac{\mathrm{d}v}{\mathrm{d}t} = -\frac{e}{m}E_0\cdot f(t)\cdot\exp(-x/l_f), \tag{19}$$

where f(t) is the normalized temporal shape of the near-field. By introducing dimensionless variables $\tilde{x} = x/l_f$, $\tilde{t} = t/T_0$ and $\tilde{v} = v\cdot T_0/l_f$, by considering the length and time scale of the equation and rearranging it, we obtain:

$$\frac{\mathrm{d}\tilde{v}}{\mathrm{d}\tilde{t}} = -\frac{e\cdot T_0^2\cdot E_0}{m\cdot l_f}\cdot f(\tilde{t})\cdot\exp(-\tilde{x}) = -\frac{4\pi^2}{\delta_{\mathrm{sf}}}\cdot f(\tilde{t})\cdot\exp(-\tilde{x}). \tag{20}$$

The strong field adiabaticity parameter δ_{sf} is the only parameter in a dimensionless equation and therefore determines the strong-field dynamics.

The final expressions appear similar, the decay length of the field is related to the length scale of electron motion. We can therefore define a generalized adiabaticity parameter δ_{nf} of electron dynamics in inhomogeneous near-fields as:

$$\delta_{\mathrm{nf}} = \frac{l_f}{l_{T_0}}, \tag{21}$$

where l_f is the near-field decay length as above and l_{T_0} is the distance an electron travels during an optical cycle. We can consider the adiabaticity parameter of attosecond streaking and of strong-field to be different realizations of the same generalized adiabaticity parameter. However, we want to point out that two very different dynamics are described. In the latter case electrons move on oscillatory trajectories and depending on the subcycle emission time might be recolliding with the surface. By contrast in the former case, they move on quasi straight trajectories. Although it might be surprising that the electron dynamics can be described by the same generalized parameter, we note that it comes out very naturally since it connects the only two relevant length scales of the problem.

References

[1] T. Brabec and F. Krausz, "Intense few-cycle laser fields: Frontiers of nonlinear optics," *Rev. Mod. Phys.*, vol. 72, pp. 545–591, Apr. 2000. [Online]. Available: http://link.aps.org/doi/10.1103/RevModPhys.72.545

[2] G. Steinmeyer, D. H. Sutter, L. Gallmann, N. Matuschek, and U. Keller, "Frontiers in ultrashort pulse generation: Pushing the limits in linear and nonlinear optics," *Science*, vol. 286, no. 5444, pp. 1507–1512, 1999. [Online]. Available: http://science.sciencemag.org/content/286/5444/1507

[3] G. G. Paulus *et al.*, "Absolute-phase phenomena in photoionization with few-cycle laser pulses," *Nature*, vol. 414, pp. 182–184, Nov. 2001.

[4] A. Baltuška *et al.*, "Attosecond control of electronic processes by intense light fields," *Nature*, vol. 421, pp. 611–615, Feb. 2003.

[5] F. Krausz and M. Ivanov, "Attosecond physics," *Rev. Mod. Phys.*, vol. 81, pp. 163–234, Jan. 2009.

[6] L. Plaja, R. Torres, and A. Zaïr, *Attosecond Physics: Attosecond Measurements and Control of Physical Systems* (Springer Series in Optical Sciences). Berlin, Germany: Springer, 2013. [Online]. Available: https://books.google.de/books?id=jPi5BQAAQBAJ

[7] U. Thumm *et al.*, *Attosecond Physics: Attosecond Streaking Spectroscopy of Atoms and Solids*. Hoboken, NJ, USA: Wiley, 2015. doi: 10.1002/9781119009719.ch13.

[8] Z. Chang, P. B. Corkum, and S. R. Leone, "Attosecond optics and technology: Progress to date and future prospects," *J. Opt. Soc. Amer. B*, vol. 33, no. 6, pp. 1081–1097, Jun. 2016.

[9] P. Hommelhoff and M. F. Kling, *Attosecond Nanophysics*. Weinheim, Germany: Wiley-VCH, 2015.

[10] M. F. Ciappina *et al.*, "Attosecond physics at the nanoscale," Jul. 2016, arXiv.

[11] E. Goulielmakis *et al.*, "Attosecond control and measurement: Lightwave electronics," *Science*, vol. 317, no. 5839, pp. 769–775, 2007. [Online]. Available: http://science.sciencemag.org/content/317/5839/769

[12] M. Krüger, M. Schenk, and P. Hommelhoff, "Attosecond control of electrons emitted from a nanoscale metal tip," *Nature*, vol. 475, pp. 78–81, Jul. 2011.

[13] A. Schiffrin *et al.*, "Optical-field-induced current in dielectrics," *Nature*, vol. 493, pp. 70–74, Mar. 2013.

[14] M. Schultze *et al.*, "Controlling dielectrics with the electric field of light," *Nature*, vol. 493, pp. 75–78, Mar. 2013.

[15] J. Itatani *et al.*, "Attosecond streak camera," *Phys. Rev. Lett.*, vol. 88, no. 17, Apr. 2002, Art. no. 173903.

[16] M. I. Stockman, M. F. Kling, U. Kleineberg, and F. Krausz, "Attosecond nanoplasmonic-field microscope," *Nature Photon.*, vol. 1, pp. 539–544, Sep. 2007.

[17] R. Kienberger *et al.*, "Atomic transient recorder," *Nature*, vol. 427, pp. 817–821, Feb. 2004.

[18] E. Skopalová *et al.*, "Numerical simulation of attosecond nanoplasmonic streaking," *New J. Phys.*, vol. 13, no. 8, Aug. 2011, Art. no. 083003.

[19] F. Süßmann and M. F. Kling, "Attosecond nanoplasmonic streaking of localized fields near metal nanospheres," *Phys. Rev. B*, vol. 84, no. 12, Sep. 2011, Art. no. 121406.

[20] A. G. Borisov, P. M. Echenique, and A. K. Kazansky, "Attostreaking with metallic nano-objects," *New J. Phys.*, vol. 14, no. 2, Feb. 2012. Art. no. 023036.

[21] F. Kelkensberg, A. F. Koenderink, and M. J. J. Vrakking, "Attosecond streaking in a nano-plasmonic field," *New J. Phys.*, vol. 14, no. 9, Sep. 2012, Art. no. 093034.

[22] J. S. Prell, L. J. Borja, D. M. Neumark, and S. R. Leone, "Simulation of attosecond-resolved imaging of the plasmon electric field in metallic nanoparticles," *Annalen der Physik*, vol. 525, pp. 151–161, Feb. 2013.

[23] M. Lupetti, J. Hengster, T. Uphues, and A. Scrinzi, "Attosecond photoscopy of plasmonic excitations," *Phys. Rev. Lett.*, vol. 113, no. 11, Sep. 2014, Art. no. 113903.

[24] G. Herink, D. R. Solli, M. Gulde, and C. Ropers, "Field-driven photoemission from nanostructures quenches the quiver motion," *Nature*, vol. 483, pp. 190–193, 2012.

[25] B. Förg *et al.*, "Attosecond nanoscale near-field sampling," *Nature Commun.*, vol. 7, May 2016, Art. no. 11717.

[26] L. Wimmer *et al.*, "Terahertz control of nanotip photoemission," *Nature Phys.*, vol. 10, pp. 432–436, 2014.

[27] J. Schäfer, S.-C. Lee, and A. Kienle, "Calculation of the near fields for the scattering of electromagnetic waves by multiple infinite cylinders at perpendicular incidence," *J. Quant. Spectrosc. Radiat. Transf.*, vol. 113, pp. 2113–2123, 2012.

[28] L. Novotny and B. Hecht, *Principles of Nano-Optics*. Cambridge, U.K.: Cambridge Univ. Press, 2006.

[29] P. B. Johnson and R. W. Christy, "Optical constants of the noble metals," *Phys. Rev. B*, vol. 6, pp. 4370–4379, Dec. 1972. [Online]. Available: http://link.aps.org/doi/10.1103/PhysRevB.6.4370

[30] C. F. Bohren and D. R. Huffman, *Absorption and Scattering of Light by Small Particles*. Weinheim, Germany: Wiley-VCH Verlag, 2007. doi: 10.1002/9783527618156.fmatter.

[31] A. L. Cavalieri *et al.*, "Attosecond spectroscopy in condensed matter," *Nature*, vol. 449, pp. 1029–1032, Oct. 2007.

[32] M. Schultze *et al.*, "Delay in photoemission," *Science*, vol. 328, no. 5986, pp. 1658–1662, 2010. [Online]. Available: http://science.sciencemag.org/content/328/5986/1658

[33] S. Neppl *et al.*, "Attosecond time-resolved photoemission from core and valence states of magnesium," *Phys. Rev. Lett.*, vol. 109, no. 8, Aug. 2012, Art. no. 087401.

[34] R. Pazourek, S. Nagele, and J. Burgdörfer, "Attosecond chronoscopy of photoemission," *Rev. Mod. Phys.*, vol. 87, pp. 765–802, Aug. 2015. [Online]. Available: http://link.aps.org/doi/10.1103/RevModPhys.87.765

[35] J. Dahlström *et al.*, "Theory of attosecond delays in laser-assisted photoionization," *Chem. Phys.*, vol. 414, pp. 53–64, 2013. [Online]. Available: http://www.sciencedirect.com/science/article/pii/S0301010412000298

[36] P. M. Paul *et al.*, "Observation of a train of attosecond pulses from high harmonic generation," *Science*, vol. 292, no. 5522, pp. 1689–1692, 2001. [Online]. Available: http://science.sciencemag.org/content/292/5522/1689

[37] K. Klünder *et al.*, "Probing single-photon ionization on the attosecond time scale," *Phys. Rev. Lett.*, vol. 106, Apr. 2011, Art. no. 143002. [Online]. Available: http://link.aps.org/doi/10.1103/PhysRevLett.106.143002

[38] M. Huppert, I. Jordan, D. Baykusheva, A. von Conta, and H. J. Wörner, "Attosecond delays in molecular photoionization," *Phys. Rev. Lett.*, vol. 117, Aug. 2016, Art. no. 093001. [Online]. Available: http://link.aps.org/doi/10.1103/PhysRevLett.117.093001

[39] R. Locher *et al.*, "Energy-dependent photoemission delays from noble metal surfaces by attosecond interferometry," *Optica*, vol. 2, no. 5, pp. 405–410, May 2015. [Online]. Available: http://www.osapublishing.org/optica/abstract.cfm?URI=optica-2-5-405

[40] J. Feist *et al.*, "Time delays for attosecond streaking in photoionization of neon," *Phys. Rev. A*, vol. 89, Mar. 2014, Art. no. 033417. [Online]. Available: http://link.aps.org/doi/10.1103/PhysRevA.89.033417

[41] C.-H. Zhang and U. Thumm, "Attosecond photoelectron spectroscopy of metal surfaces," *Phys. Rev. Lett.*, vol. 102, Mar. 2009, Art. no. 123601. [Online]. Available: http://link.aps.org/doi/10.1103/PhysRevLett.102.123601

[42] C. Lemell, B. Solleder, K. Tőkési, and J. Burgdörfer, "Simulation of attosecond streaking of electrons emitted from a tungsten surface," *Phys. Rev. A*, vol. 79, Jun. 2009, Art. no. 062901. [Online]. Available: http://link.aps.org/doi/10.1103/PhysRevA.79.062901

[43] A. K. Kazansky and P. M. Echenique, "One-electron model for the electronic response of metal surfaces to subfemtosecond photoexcitation," *Phys. Rev. Lett.*, vol. 102, Apr. 2009, Art. no. 177401. [Online]. Available: http://link.aps.org/doi/10.1103/PhysRevLett.102.177401

[44] E. E. Krasovskii, "Attosecond spectroscopy of solids: Streaking phase shift due to lattice scattering," *Phys. Rev. B*, vol. 84, Nov. 2011, Art. no. 195106. [Online]. Available: http://link.aps.org/doi/10.1103/PhysRevB.84.195106

[45] C.-H. Zhang and U. Thumm, "Probing dielectric-response effects with attosecond time-resolved streaked photoelectron spectroscopy of metal surfaces," *Phys. Rev. A*, vol. 84, Dec. 2011, Art. no. 063403. [Online]. Available: http://link.aps.org/doi/10.1103/PhysRevA.84.063403

[46] A. G. Borisov, D. Sánchez-Portal, A. K. Kazansky, and P. M. Echenique, "Resonant and nonresonant processes in attosecond streaking from metals," *Phys. Rev. B*, vol. 87, Mar. 2013, Art. no. 121110. [Online]. Available: http://link.aps.org/doi/10.1103/PhysRevB.87.121110

[47] S. Neppl *et al.*, "Direct observation of electron propagation and dielectric screening on the atomic length scale," *Nature*, vol. 517, pp. 342–346, Jan. 2015.

[48] S. Tanuma, S. Ichimura, K. Goto, and T. Kimura, "Experimental determinations of electron inelastic mean free paths in silver, gold, copper and silicon from electron elastic peak intensity ratios," *J. Surf. Anal.*, vol. 9, no. 3, pp. 285–290, 2002.

[49] W. A. Okell *et al.*, "Temporal broadening of attosecond photoelectron wavepackets from solid surfaces," *Optica*, vol. 2, no. 4, pp. 383–387, Apr. 2015. [Online]. Available: http://www.osapublishing.org/optica/abstract.cfm?URI=optica-2-4-383

[50] M. Lucchini *et al.*, "Light-matter interaction at surfaces in the spatiotemporal limit of macroscopic models," *Phys. Rev. Lett.*, vol. 115, Sep. 2015, Art. no. 137401. [Online]. Available: http://link.aps.org/doi/10.1103/PhysRevLett.115.137401

[51] T. Fuji *et al.*, "Monolithic carrier-envelope phase-stabilization scheme," *Opt. Lett.*, vol. 30, no. 3, pp. 332–334, Feb. 2005. [Online]. Available: http://ol.osa.org/abstract.cfm?URI=ol-30-3-332

[52] M. Eisele, M. Krüger, M. Schenk, A. Ziegler, and P. Hommelhoff, "Note: Production of sharp gold tips with high surface quality," *Rev. Scientific Instrum.*, vol. 82, no. 2, Feb. 2011, Art. no. 026101.

[53] J. G. Fujimoto, J. M. Liu, E. P. Ippen, and N. Bloembergen, "Femtosecond laser interaction with metallic tungsten and nonequilibrium electron and lattice temperatures," *Phys. Rev. Lett.*, vol. 53, pp. 1837–1840, Nov. 1984. [Online]. Available: http://link.aps.org/doi/10.1103/PhysRevLett.53.1837

[54] A. M. Summers *et al.*, "Optical damage threshold of Au nanowires in strong femtosecond laser fields," *Opt. Express*, vol. 22, no. 4, pp. 4235–4246, Feb. 2014. [Online]. Available: http://www.opticsexpress.org/abstract.cfm?URI=oe-22-4-4235

[55] L. Wu and L. K. Ang, "Nonequilibrium model of ultrafast laser-induced electron photofield emission from a dc-biased metallic surface," *Phys. Rev. B*, vol. 78, Dec. 2008, Art. no. 224112. [Online]. Available: http://link.aps.org/doi/10.1103/PhysRevB.78.224112

[56] H. Yanagisawa *et al.*, "Energy distribution curves of ultrafast laser-induced field emission and their implications for electron dynamics," *Phys. Rev. Lett.*, vol. 107, Aug. 2011, Art. no. 087601. [Online]. Available: http://link.aps.org/doi/10.1103/PhysRevLett.107.087601
[57] C. Lemell *et al.*, "Real-time observation of collective excitations in photoemission," *Phys. Rev. B*, vol. 91, Jun. 2015, Art. no. 241101. [Online]. Available: http://link.aps.org/doi/10.1103/PhysRevB.91.241101
[58] A. Feist *et al.*, "Quantum coherent optical phase modulation in an ultrafast transmission electron microscope," *Nature*, vol. 521, pp. 200–203, May 2015.
[59] S. V. Yalunin, B. Schröder, and C. Ropers, "Theory of electron energy loss near plasmonic wires, nanorods, and cones," *Phys. Rev. B*, vol. 93, Mar. 2016, Art. no. 115408. [Online]. Available: http://link.aps.org/doi/10.1103/PhysRevB.93.115408
[60] J. Gagnon, E. Goulielmakis, and V. Yakovlev, "The accurate frog characterization of attosecond pulses from streaking measurements," *Appl. Phys. B*, vol. 92, no. 1, pp. 25–32, 2008. doi: 10.1007/s00340-008-3063-x.

Johannes Schötz received the M.Sc. degree in physics, in 2014, from Ludwig-Maximilians-Universität München, Munich, Germany, where he is currently working toward the Ph.D. degree in the Ultrafast Nanophotonics Group of Prof. M. Kling.

His research interests include nanoplasmonics, attosecond nanophysics, and strong-field physics.

Benjamin Förg was born in Neuburg, Germany, in 1987. He received the M.Sc. degree in physics from the University of Augsburg, Augsburg, Germany. In 2013, he joined the Ultrafast Nanophotonics Group, Max-Planck-Institute of Quantum Optics, Garching, Germany, where he is currently working toward the Ph.D. degree.

His research interests include ultrafast electron dynamics in gases and molecular compounds, the generation of high-fluence extreme ultraviolet pulses, attosecond nanophysics, and potential applications in light-driven nanoelectronics.

Michael Förster received the M.Sc. degree in physics from Julius-Maximilians-Universität Würzburg, Würzburg, Germany, and the Ph.D. degree in physics from Ludwig-Maximilians-Universität München, Munich, Germany, in 2016.

He is currently working as a Postdoctoral Researcher in the group of Prof. P. Hommelhoff at the Friedrich-Alexander Universität Erlangen-Nürnberg, Erlangen, Germany. His research interests include attosecond nanophysics, ultrafast laser physics, strong-field physics, and ultrafast electron sources.

William A. Okell received the M.A. degree in natural sciences from the University of Cambridge, Cambridge, U.K., in 2008, the M.Sc. degree in physics from Imperial College London, London, U.K., in 2010, and the Ph.D. degree in ultrafast laser physics from Imperial College London, in 2014, in the group of Prof. J. W. G. Tisch and Prof. J. P. Marangos.

He was as a Postdoctoral Researcher with Imperial College London and, from 2015, with the Max-Planck-Institute of Quantum Optics, Garching, Germany. His research interests include attosecond surface science, ultrafast nanoplasmonics, and few-cycle femtosecond pulse generation.

Dr. Okell received the EPSRC Doctorial Prize Fellowship (U.K., 2014).

Mark I. Stockman received the Diploma in physics and the M.Sc. degree in theoretical physics, in 1970, from Novosibirsk State University, Novosibirsk, Russia, and the Ph.D. degree in theoretical physics from the Institute of Nuclear Physics, Russian Academy of Sciences, Novosibirsk, Russia, in 1975.

Since 1996, he has been a Professor of physics at Georgia State University, Atlanta, GA, USA, where he became the Director of the Center for Nano-Optics in 2014. From 2007 to 2014, he spent several stays as a Guest Professor at the Ludwig-Maximilians Universität München, Munich, Germany and the Max-Planck Institute of Quantum Optics, Garching, Germany. He is the author of more than 190 major research articles. His current research focuses on electronic and optical properties of plasmonic metal and metal-semiconductor nanostructures.

Prof. Stockman is a Fellow of the American Physical Society, the Optical Society of America, and The International Society for Optical Engineering. He is currently holding several grants from the US Department of Energy and the US Department of Defense.

Ferenc Krausz was born in Mór, Hungary, in 1962. He received the Diploma in electrical engineering from the University of Technology, Budapest, Hungary, in 1985, and the Ph.D. degree in laser physics from the Department of Electrical Engineering, University of Technology, Vienna, Austria, in 1991.

He became an Assistant Professor in 1996 and the Full Professor in 1999 at the University of Technology, Vienna. Since 2004, he has been the Professor and Chair of the Department of Experimental Physics—Laser Physics, Ludwig-Maximilians-Universität München, Munich, Germany, and the Director in the Max-Planck-Institute of Quantum Optics, Garching, Germany. He is the Director of the Munich-Centre for Advacned Photonics, the Laboratory for Extreme Photonics, and the Centre for Advanced Laser Applications.

Prof. Krausz is the member of the Austrian Academy of Science (Austria, 2003), the Hungarian Academy of Sciences (Hungary, 2007), the European Academy of Sciences and Arts (Austria, 2007), the Russian Academy of Sciences (Russia, 2011), the European Academy of Sciences (Belgium, 2012), the Academia Europaea (U.K., 2012), and of the Leopoldina, the National Academy of Germany (Germany, 2016). He received several major awards including the Carl Zeiss Award (Germany, 1998), the King Faisal International Prize for Science (Saudi Arabia, 2013), and the Otto-Hahn-Prize (Germany, 2013). He became the Thomson Reuters Citation Laureate in Physics in 2015. He holds the Order of Merit of the Federal Government (Germany, 2011) and the Knight's Cross of the Order of Merit of Hungary (Hungary, 2012).

Peter Hommelhoff received the Diploma in physics from the Swiss Federal Institute of Technology, Zürich, Switzerland, in 1999, and the Ph.D. degree from Ludwig-Maximilians-Universität München, Munich, Germany, in 2002, in the group of Prof. T. W. Hänsch.

He was a Postdoctoral Researcher in the group of Prof. M. Kasevich at Stanford University, Stanford, CA, USA, and later became a Group Leader in the Max-Planck-Institute of Quantum Optics, Garching, Germany. Since 2012, he has been a Professor at Friedrich-Alexander Universität Erlangen-Nürnberg, Erlangen, Germany, and holds the Chair for laser physics. Together with Matthias Kling, he is an Editor of the book *Attosecond Nanophysics* (Wiley, 2015).

Prof. Hommelhoff received several awards including an ERC Consolidator Grant (EU, 2014).

Matthias F. Kling studied physics at Georg-August-University, Göttingen, Germany, and laser physics at Friedrich-Schiller University, Jena, Germany. He received the Diploma and Ph.D. degree from Georg-August-University, in 1998 and 2002, respectively, in physics.

His postdoctorial research experience include stays in the group of Prof. C. B. Harris, University of California–Berkeley, Berkeley, CA, USA and in the group of Prof. M. J. J. Vrakking, FOM Institute for Atomic and Molecular Physics, Amsterdam, The Netherlands. In 2007, he became the Research Group Leader in the Max-Planck-Institute of Quantum Optics, Garching, Germany. From 2009 to 2013, he was an Assistant Professor at Kansas State University, Manhattan, KS, USA. Since 2013, he has been a Professor at Ludwig-Maximilians-Universität München, Munich, Germany and Heads the Ultrafast Nanophotonics Group, which is part of the Laboratory of Attosecond Physics at MPQ and LMU. Together with Peter Hommeloff he is an Editor of the book *Attosecond Nanophysics* (Wiley, 2015).

Prof. Kling received several awards including the Röntgen prize by the University of Giessen (2011), the Nernst-Haber-Bodenstein prize by the German Bunsen Society (2012), an Early Career Award by the Department of Energy (USA, 2012), and an ERC Starting Grant by the European Union (2013).